Boron shielding design for neutron and gamma detectors of a pulsed neutron tool*

Xin-Yang Wang,[1] Jun-Yan Chen,[1] and Qiong Zhang[1,†]

[1] *University of Electronic Science and Technology of China, Chengdu 611731, China*

Shielding material is critical for downhole pulsed neutron tool design as it directly influences the accuracy of formation measurements. A well-designed shield configuration ensures that the response of the tool is maximally representative of formation without being impacted by tool and borehole environment. This manuscript investigates the effects of boron-containing materials on neutron and gamma detectors based on a newly designed logging-while-drilling tool, which is currently undergoing manufacturing process. As boron content increases, its ability to absorb thermal neutrons significantly enhances. Through simulation, it is proven that boron carbide (B_4C)can be used as an effective boron shielding material for thermal neutrons and therefore employed in this work. To shield against thermal neutrons migrating from mud pipes, the optimal shielding thicknesses for near and far neutron detectors are determined to be 5mm and 4mm. At a porosity of 25 p.u., the near neutron sensitivity shows a 5.6% increase in response. Furthermore, in order to shield capture gamma generated by thermal neutrons once they enter tool from the mud pipe and formation, the internal and external shields for the gamma detector are evaluated. Results show internal shield needs 75% boron content while the external shield is of 14.2mm thickness and 25% boron content to minimize tool effect.

Keywords: Nuclear well logging, Pulsed neutron tool, Boron shielding

I. INTRODUCTION

In the process of petroleum exploration and development, using chemical source in nuclear well logging is a commonly used method. This technique employs Cs137 or AmBe sources to assess formation properties [1, 2]. However, concerns persist about the environmental pollution risks posed by chemical sources during their transportation and measurement. Consequently, pulsed neutron well logging, noted for its safety and controllability, has emerged as a viable alternative to traditional well logging.

Pulsed neutron logging has become an indispensable method for the evaluation of complex oil and gas reservoirs. It relies on a pulsed neutron generator, which is an electronically controlled small accelerator neutron source. By adjusting pulse emission frequency, it can achieve integrated measurements [3] of multiple formation parameters, such as density, porosity, lithology [4]. Although pulsed neutron logging reduces radioactive risks and provides richer formation information through a single measurement compared to traditional well logging, the strong penetration capability of high-energy neutrons and the variable distribution of secondary gamma rays may cause mutual influence on gamma or neutron detection [5–8], especially in LWD measurements, where particles may penetrate through the mud pipes and reach the detectors directly. As a result, there may be a higher level of tool-related information mixed in the detector recorded information, therefore reduce the proportion of formation response. In order to reduce non-formation-related information, it is necessary to study the tool shielding design. To understand the rationale behind the shielding design, it is necessary to first review the principles of pulsed neutron logging.

* Supported by the Natural Science Foundation of China U23B20151 and 52171253)

† Corresponding author, Qiong Zhang, University of Electronic Science and Technology of China, Chengdu 611731, China (e-mail: zhanqio@uestc.edu.cn)

A. Overview of pulsed neutron well logging principle

In pulsed neutron logging, taking a D-T source as an example, after the emission of 14MeV fast neutrons, the initial energy loss of the neutrons occurs most due to inelastic collision interactions [9]. During the process of neutron deceleration, multiple inelastic collisions may occur, resulting in inelastic scattering rays with characteristic energies specific to different elements. As fast neutrons decelerate to thermal neutrons and are absorbed by target nuclei in geological formations, characteristic energy capture gamma rays are emitted. By analyzing the energy spectra of these two types of gamma rays, the elemental composition of geological formations can be determined [10].

Simultaneously, as neutron energy decreases, elastic collisions gradually become the dominant reaction process in neutron deceleration. In elastic collisions, the energy of the neutron is transferred to the target nucleus in a manner consistent with conservation of kinetic energy within the system as Eq. 1.

$$E_M = E_n - E_n' = \frac{4Mm}{(M+m)^2} E_n cos\theta^2. \tag{1}$$

The kinetic energy of the recoil nucleus is denoted as E_M, the kinetic energy of the neutron before collision is E_n, and the kinetic energy after collision is E_n'. The masses of the recoil nucleus and the neutron are represented by m and M, respectively. The angle between the recoil nucleus and the incident neutron direction is θ. Therefore, when neutrons collide head-on with hydrogen atoms, they experience maximum energy loss. Hydrogen is commonly found in formations in the form of water, oil, gas, and other substances. When neutrons are decelerated to thermal energies by hydrogen atoms and subsequently detected by detectors, the porosity of the formation can be inferred [4].

B. Motivation for investigating boron shielding

In the design of pulsed neutron tools, it is often necessary to incorporate several different types of detectors to enable various measurement modes within a single tool. LWD tools differ from cable tools due to the inclusion of a mud pipe, which can lead to thermal neutron leakage and subsequent generation of capture gamma rays when the tool elements capture these neutrons. To illustrate the impact of the described physical processes on downhole detection, as depicted in Fig. 1, consider a pulse neutron tool comprising one neutron detector and one gamma-ray detector, with a mud pipe. Fig. 1 outlines the potential physical pathways that particles reaching the detectors might traverse, as indicated by paths ①-⑦. For the neutron, the possible paths include ①-④. As for gamma, it summarized as paths ⑤-⑦.

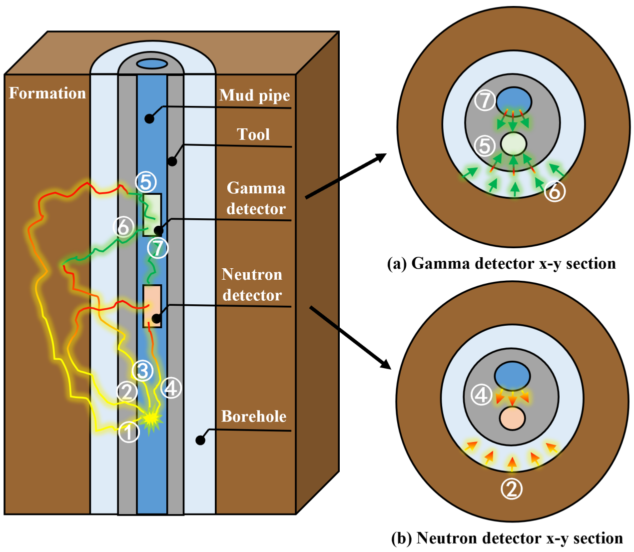

Fig. 1. Path diagram of n-γ physic reactions in pulsed neutron well logging tool

Path ① and Path ③: After the 14MeV neutrons are generated, they are moderated through the tool, the borehole, and the formation, respectively, forming thermal neutrons in the formation and subsequently in the tool. Path ②: After the 14MeV neutrons are generated from the source, they are moderated through the tool, the borehole, and the formation, after which the thermal neutrons formed are captured by the neutron detector. Path ④: Fast neutrons generated from the source may be directly moderated within the tool (including the mud pipe) and ultimately detected by neutron detectors. Path ⑤: Following path ①, the neutrons returning to the tool generate capture and inelastic gamma rays. Path ⑥: Similar to Path ⑤, but the generation of capture and inelastic gamma rays occurs within the formation. Path ⑦:The neutrons that follow path ④ result in the generation of both capture and inelastic gamma inside the tool.

In the case of Path ④, the neutrons might be detected directly without interacting with the formation, which is disadvantageous for measuring formation porosity. In the gamma paths ⑤ and ⑦, gamma rays generated within the tool (including the mud pipe) need to be shielded, especially for common tool elements like Fe, Ni, Mn, etc., whose tool-related contributions could lead to inaccuracies in determining the formation's elemental content [11–13]. This is because the tool's spectrum might overshadow the formation's information, leading to inaccuracies or incomplete subtraction of the tool's spectrum, thereby complicating elemental measurement. Therefore, one feasible approach in spectrum analysis is to reduce the contribution of tool body elemental composition [14–16]. However, once fast neutrons emitted from the tool enter formation, the generation of inelastic gamma rays is inevitable, and this portion of inelastic gamma rays produced by the tool cannot be eliminated through shielding [17]. Therefore, in element's measurement, it is crucial to shield the potential thermal neutrons that may undergo neutron capture reactions with the tool, such as by implementing shielding around the tool or mud pipe to prevent direct reactions of thermal neutrons with the tool elements.

Boron is an important element in neutron shielding as it has a high thermal neutron absorption cross-section [18, 19].Compared to other elements commonly used for neutron shielding, such as cadmium and gadolinium, boron releases relatively low gamma energy during the capture process, which can be removed by lower energy truncation. These characteristics render boron an effective shielding material element. Previous studies [20–28], have demonstrated the feasibility of using Monte Carlo simulation software for tool densign. These studies indicate that there are various materials available for thermal neutron shielding [29], including some novel materials [30–33], which exhibit gamma and neutron shielding properties and are used in applications such as shielding ionizing radiation and medical diagnostics. Additionally, materials like boron concrete, borated polyethylene [34], and boron-containing stainless steel are employed in fields like laboratory shielding [35] and nuclear power plant [36] shielding. However, high temperature and pressure in downhole environment, along with the tool volumetric constraints, bring new challenges for more effective shielding.

Nonetheless, the key challenge in well logging tool shielding lies in: firstly, the spatial limitations of the tool itself preclude the design of overly thick shielding layers to shield high-energy neutrons, necessitating materials with high shielding efficiency to achieve maximal shielding effectiveness within limited space. Secondly, when selecting appropriate shielding materials, it is essential to consider factors such as melting point, tensile strength, and hardness, etc. This enables the provision of a wider range of material options that can adapt to high-temperature environments or complex structural components of the tool.

This manuscript explores the design of boron-containing shielding for an LWD pulsed neutron tool, emphasizing its impact on neutron and gamma detection. Monte Carlo simulations are conducted to investigate the shielding materials and thicknesses of the neutron detector, aiming to ascertain its effects on neutron count rates and ratios. Additionally, the internal and external shielding of the gamma detector is being assessed to investigate its effects on gamma energy spectra

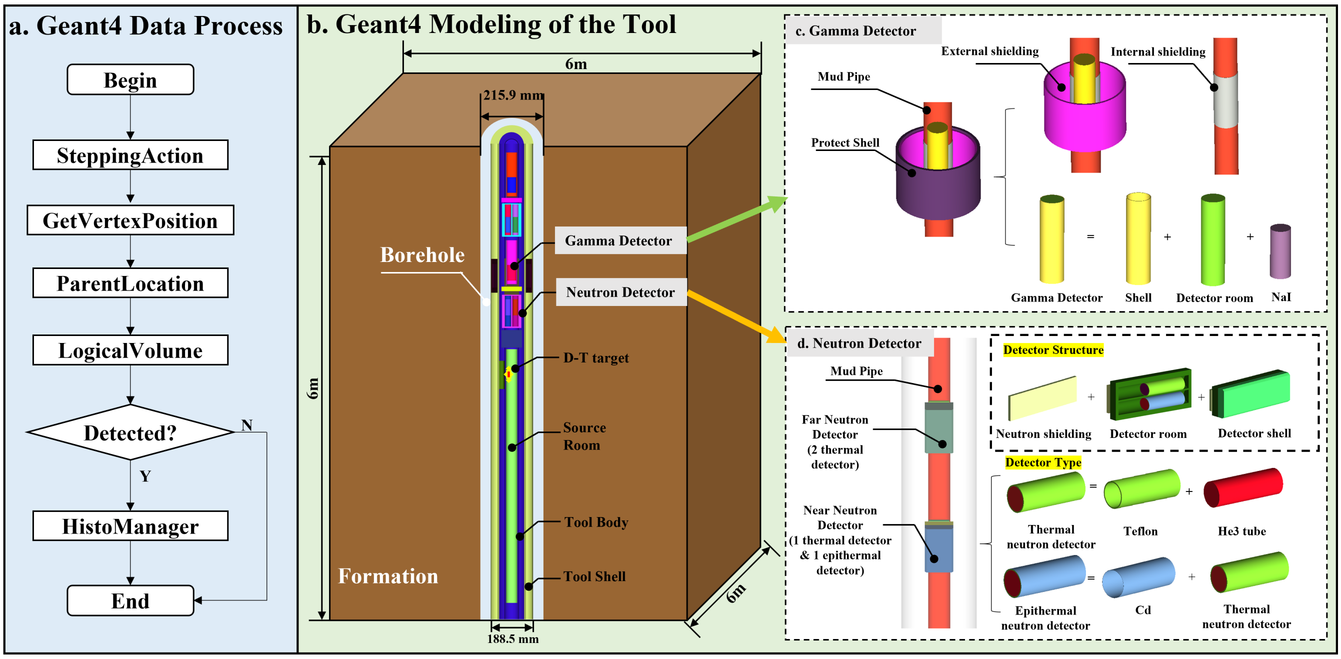

Fig. 2. Multi-detector pulsed neutron tool's construction in Geant4

and count rates. The aim of this study is to provide references for the design of shielding for pulse neutron tools.

II. PULSED NEUTRON TOOL DESIGN

A. Monte Carlo modeling of the tool

Open-source Monte Carlo simulation software Geant4 (Geometry and Tracking 4) is used for evaluation [37]. This manuscript employs a pulsed neutron logging tool which is under development. This tool can acquire critical formation parameters such as elemental composition, density, and porosity. For integrated detection, both gamma and neutron detectors are included. To simulate pulsed neutron tool detection, the source is defined as a 14MeV pulsed neutron source in Geant4. The detailed model is presented in Fig. 2.

To differentiate the origins of the particle obtained in the detector, the data process in Geant4 is illustrated in Fig. 2. During the particle transportion, the type of each particle produced is identified by calling *SteppingAction*, such as gamma produced by neutron inelastic collisions or capture reaction. Then, based on *GetVertexPosition()*, the position, or called as *logicalVolume* where the gamma were generated, is obtained, such as formations, borehole, tool, or mud pipe. If the particle reaches the detector, it is logged in *HistoManager*, enabling the subsequent output of results.

B. Shields of neutron detector

The tool incorporates an internal mud pipe primarily for transporting drilling mud during logging. After the emission of fast neutrons, thermal neutrons may travel directly to the neutron detectors via the mud pipe and therefore to shield against these neutrons, neutron shielding is typically installed at the bottom of the neutron detectors within the tool, as depicted in Fig. 2. The neutron detector is enveloped by three layers: the bottom layer is the neutron shield, the detectors are placed in the middle layer within an aluminum alloy detector room, and the top layer is an aluminum alloy detector shell.

To make boron compounds suitable for engineering applications, they must be processed into solid forms. However, boron compounds are inherently brittle and exhibit low solubility in steel, making the preparation of high-boron steel very challenging as the boron content increases. Therefore, to select the optimal shield material, this manuscript selects three materials to evaluate their impact on neutron measurements.

- **Aluminum Boron Carbide (Al-B_4C):** With a density of 2.6 g/cm^3, this composite material contains 40% B_4C and 60% aluminum. It has a hardness range of 300-400 GPa and a lower melting point range of 190-200°C. [38]
- **Boron Carbide (B_4C):** B_4C is known for its high structural strength, this material has a density of 2.52 g/cm^3 with a composition of B10 (76.9%) and C (23.1%). It exhibits a high hardness of 500 GPa and a melting point of 2350°C. [39, 40]
- **Aluminum-Boron (Al-B) Alloy:** Al-B alloys are

renowned for their high strength, excellent corrosion resistance. Selected material [41, 42] with a density of 2.45 g/cm^3, including B10 (11%), Si (0.3%), Fe (0.35%), Ti (0.08%), K (1%), Na (0.5%), and Al (86.77%). Its hardness is in the range of 100-200 GPa with a tensile strength of 220-250 MPa and a melting point between 690-700°C.

C. Shields of gamma detector

In this tool, the far gamma detector is used for density measurement, while the near gamma detector is employed for element measurement. The near gamma detector consisted of two shielding: one shields thermal neutrons migrating from the mud pipe, and the other shields thermal neutrons migrating from outside the tool, as shown in Fig. 2.

Due to the challenges in shaping pure boron and its high cost, this manuscript utilizing HNBR rubber mixed with boron for external shielding in the tool. For the structural constraints, the maximum thickness of internal shielding is 1.1mm, hence the plan to use pure boron material for internal shielding. Subsequent sections will focus on optimizing shielding for the near gamma detector, investigating the effects of different thicknesses and boron contents in both internal and external shields on spectral elemental measurements.

III. RESULTS ANALYSIS AND DISCUSSION

This section conducts a design study of the shielding based on the tool described above. To investigate the influence patterns of neutron and gamma detection in the tool, detector responses are obtained by altering the boron material and its thickness. 10^8 particles are simulated. The tool is positioned centrally within a sandstone formation.

A. Shield design of neutron detector

1. Neutron spatial distribution analysis

This section first analyzes the distribution of thermal and fast neutrons inside the mud pipe. In Geant4, the X-Z cross-section of the mud pipe is extracted as shown in Fig. 3(a) for flux analysis:

The source-to-detector distances for two neutron detectors are 28.8 cm and 69.2 cm, respectively. As shown in Fig. 3(b), the quantity of lower energy neutrons(<1MeV) decreases sharply with an increase in source-to-detector distance. In Fig. 3(c), the distribution of fast neutrons is primarily concentrated around the source; after emission, they are rapidly moderated by the surrounding media, resulting in minimal distribution within the mud pipe, the tool, and the borehole, making it difficult for them to reach the near and far neutron detectors. In contrast, thermal neutrons, as depicted in Fig. 3(d), exhibit a distribution in the mud pipe that is significantly different from that of fast neutrons. At the position

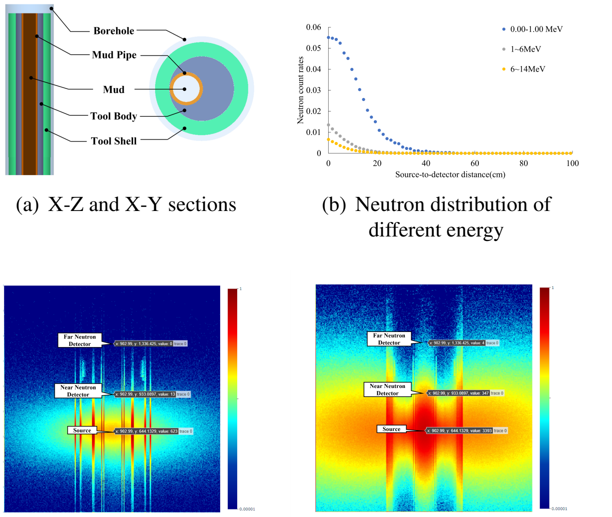

(a) X-Z and X-Y sections

(b) Neutron distribution of different energy

(c) Fast neutron distribution

(d) Thermal neutron distribution

Fig. 3. Neutron spatial distributions

of the near neutron detector, the thermal neutron, originating from the mud pipe, decreases by approximately 9.7 times. Without adequate shielding, the near neutron detector would be significantly affected. In contrast, the far-source neutron detector is less influenced.Since the thermal neutrons inside the mud pipe are not influenced by the external environment, different shielding designs can be employed for detectors at varying source-to-detector.

2. Material comparison

This section analyzes the performance of three shielding materials, B_4C, Al-B_4C, and Al-B alloy, focusing on the near neutron count rate, near epithermal neutron count rate, far neutron count rate, and the neutron ratio (the ratio of the near detector count rate to the far detector count rate) under different porosities, as shown in Fig. 4. For neutron porosity measurement, the detection sensitivity S is defined as Eq. 2.

$$S = \frac{\partial R}{R \partial \emptyset}. \tag{2}$$

The thermal neutron count ratio is defined as R; the formation porosity is $\emptyset$. At the location of far neutron detector as Fig. 4(b), thermal neutron flux is relatively low, indicating that fewer neutrons are received from the mud pipe and thermal neutron count is predominantly influenced by formation. Therefore, as the porosity changes, far neutron detector counts are comparable across the three materials. However, as shown in Fig. 4(a), the near detector is more significantly affected by thermal neutrons from within the mud pipe. Among the materials, the AlB alloy has the lowest boron content at 11%, while B_4C has the highest at 76%, making B_4C the most capable in absorbing thermal neutrons. Consequently, under

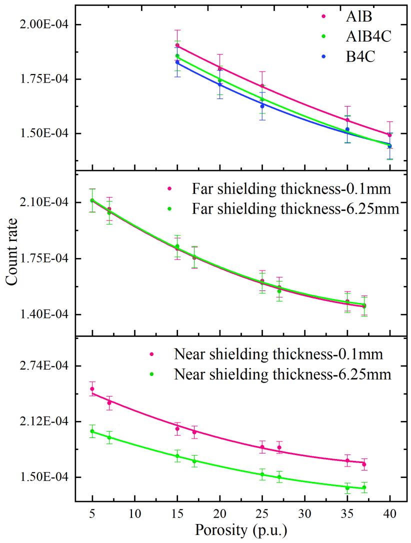

(a) Near neutron detector

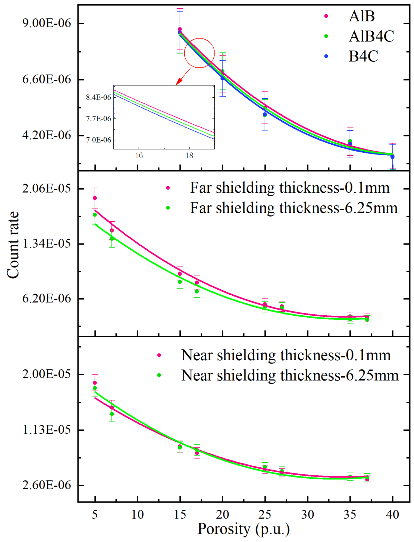

(b) Far neutron detector

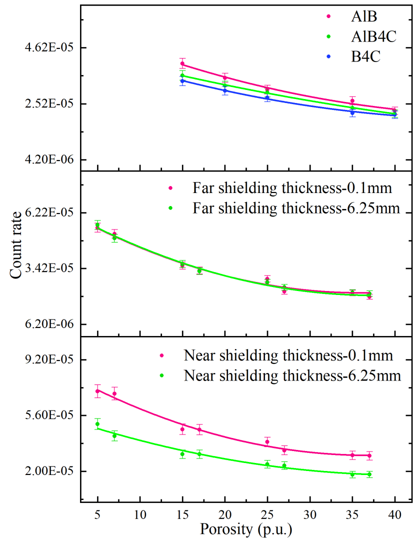

(c) Thermal neutron detector

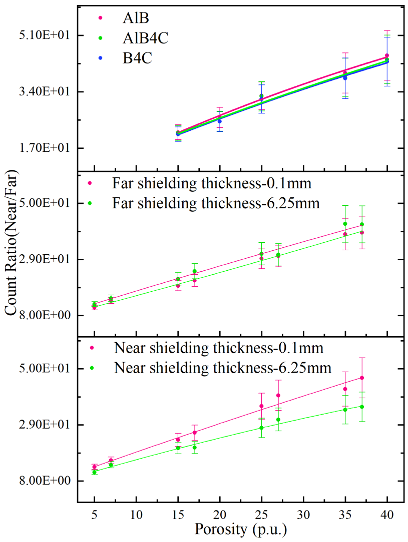

(d) Count Ratio

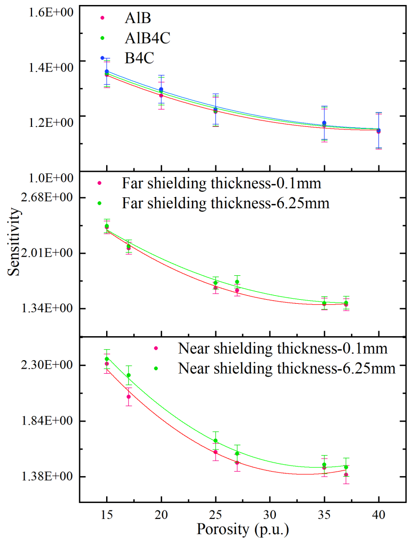

(e) Sensitivity

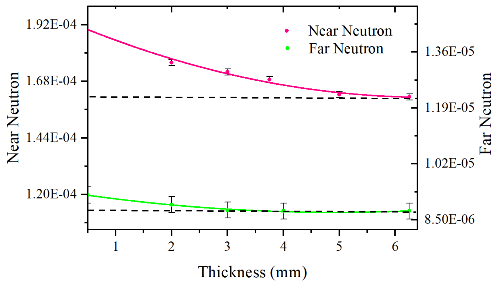

(f) Near and far neutron count rate with various thickness

Fig. 4. Comprehensive analysis of neutron measurements under various conditions

B_4C shielding, the count rate for near thermal neutrons and epithermal neutrons is the lowest as Fig. 4(c). Although the AlB alloy has a higher near source count rate, resulting in a larger detector ratio, it can be seen from Fig. 4(e) that the AlB alloy has the lowest sensitivity, whereas B_4C achieves the highest sensitivity response.

The reason for this phenomenon is that when using low boron content shielding, the detector receives overwhelm-

ing non-formation information. Therefore, it is no longer sensitive to formation parameters when formation porosity changes. The recommended materials in this manuscript are still B_4C and Al-B_4C. From the trend of near detector counts change in porosity, B_4C exhibits the best shielding performance, whereas Al-B_4C follows, making it a viable alternative to B_4C.

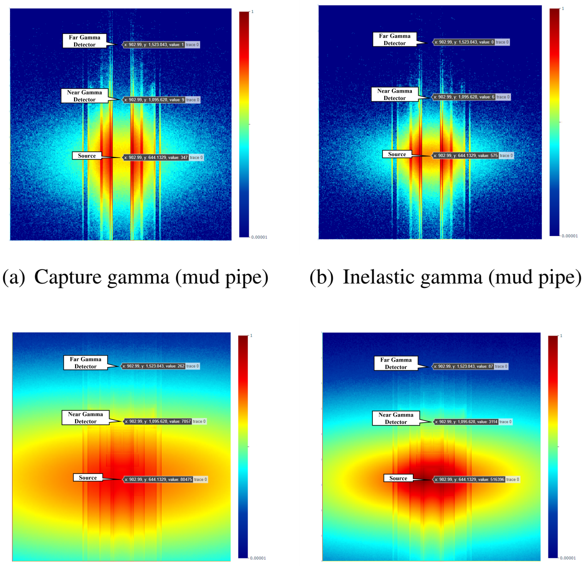

(a) Capture gamma (mud pipe) (b) Inelastic gamma (mud pipe)

(c) Capture gamma (tool) (d) Inelastic gamma (tool)

Fig. 5. Gamma spatial distribution

3. *The effect of shielding thickness*

With B4C identified as the best shielding material, its effectiveness was evaluated at various thicknesses to observe changes in the neutron detector count rate. Fig. 4 shows a comparison of the near and far neutron detectors at different shielding thicknesses. It is observed that changes in the shielding of one detector do not affect the counting pattern of the other detector. For detectors at two source distances, as porosity increases, the formation's capacity to moderate neutrons enhances, leading to a shorter moderation length and consequently fewer neutrons returning to the detectors. The overall count rate decreases. Neutrons transmitted through the mud pipe are unaffected by the environment, so their count remains constant. In the near neutron detector, as shown in Fig. 4(a), changing the shielding thickness results in a noticeable reduction in counts. For the far neutron detector, as shown in Fig.4(b), the differences gradually diminish with increasing porosity and tend to converge. This convergence is due to the increasing proportion of non-formation information when formation information is reduced, potentially preventing the far detector from accurately identifying formation information at high porosities.

The sensitivity variations of the near and far detectors at different thicknesses are shown in Fig. 4(e). It can be seen that the thicker the shielding, the lower the sensitivity. For example, at a porosity of 25p.u., the sensitivities of the near detector shielding with thicknesses of 0.1mm and 6.25mm are 1.58 and 1.67, respectively, indicating a 5.6% increase in sensitivity response.Fig.4(f) illustrates the count rate variations for both detectors at different shielding thicknesses. It is noted that the count rate for the far detector gradually stabilizes at a shielding thickness of 4mm. The neutron contribution at this part is mostly from the tool background and the formation contribution. In contrast, the count rate for the near neutron detector stabilizes at 5mm. Therefore, for the shielding design of these neutrons, the near neutron detector is set at a 5mm thickness, while the far neutron detector is set at 4mm.

B. Shield design of gamma detector

1. *Gamma spatial distribution analysis*

To design the optimal gamma shield, it is equally necessary to understand the distribution of gamma rays. Inelastic gamma rays are generated by high-energy neutrons through inelastic collisions, while capture gamma rays are produced by the capture of thermal neutrons. Therefore, after neutrons passing through the mud pipe and the tool, they will generate gamma information unrelated to the formation. Fig. 5(a) and Fig. 5(b) show the distribution of capture and inelastic gamma rays generated within mud pipe, while Fig. 5(c) and Fig. 5(d) show the distribution of capture and inelastic gamma rays generated within the tool.

The source-to-detector distances for the gamma detectors are 45.1 cm and 87.8 cm, respectively. Within the mud pipe, as depicted in Fig. 5(a) and Fig. 5(b), the distribution of capture gamma rays is broader, while inelastic gamma rays are primarily congregated near the source. Additionally, combining this with Fig. 3(d), it is evident that there are not many capture gamma rays originating from the mud pipe. This is because the probability of hydrogen elements within the mud pipe undergoing capture reactions is lower than that of the metal elements inside the tool. However, as shown in Fig. 5(c) and Fig. 5(d), a significant amount of capture gamma rays and inelastic gamma rays are generated inside the tool. Regarding the capture gamma flux, the attenuation at the near gamma detector is approximately 11.4 times that at the source, while the inelastic gamma rays decrease by 165 times. The attenuation of capture gammas is less significant than that of inelastic gammas. Therefore, it is necessary to block the thermal neutrons passing through the mud pipe and those about to react with the tool in order to reduce the contribution of tool-related capture gammas.

2. *The effect of boron content*

To investigate the impact of boron shielding on gamma detection, this section initially examines the variations in gamma count rates and energy spectra across shields with

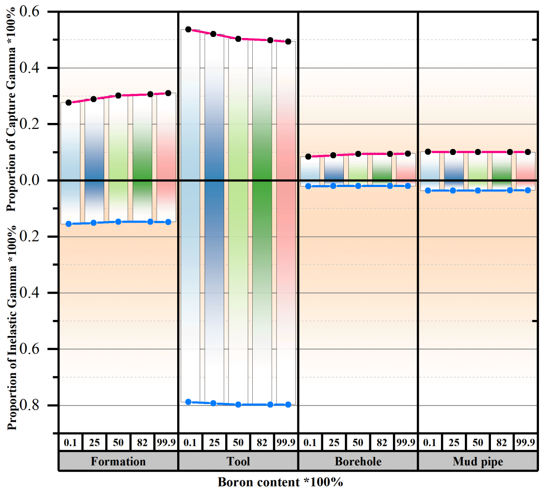

(a) Gamma count with different boron contents of internal shield

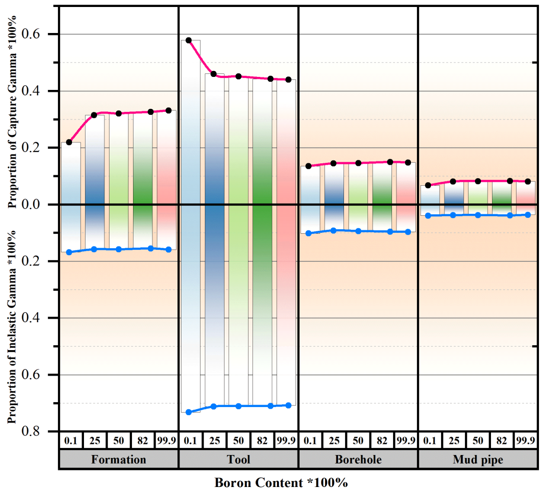

(b) Gamma count with different boron contents of external shield

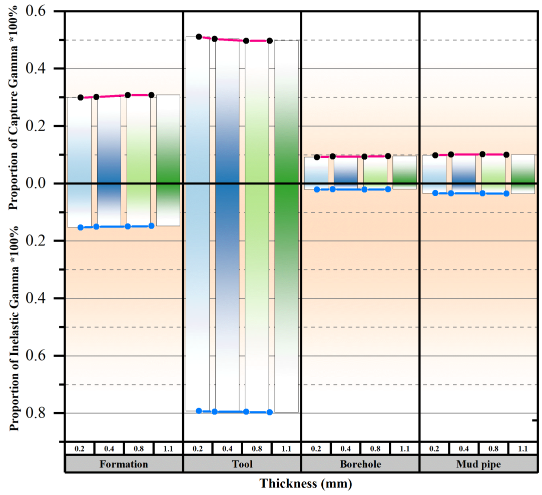

(c) Gamma count with different shielding thickness of internal shield

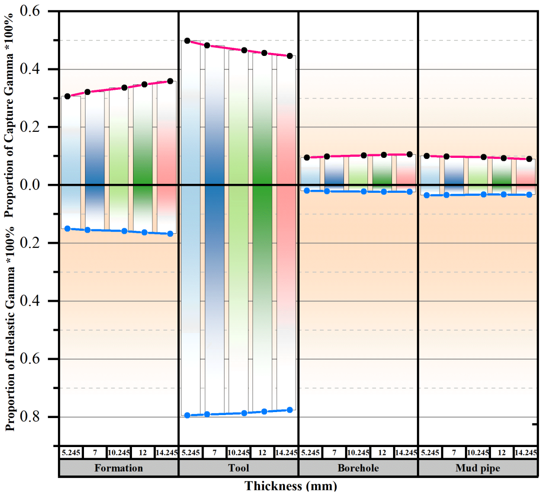

(d) Gamma count with different shielding thickness of external shield

Fig. 6. Comprehensive analysis of gamma measurements under various conditions

varying boron contents of 0.1%-99.9%. Set the thickness of the external shielding to 10 mm and the internal shielding thickness to 1 mm. Fig. 6 illustrates the changes in the proportional contributions of capture and inelastic gamma rays originating from the formation, tool, mud pipe, and borehole. The gamma contribution from the tool constitutes a significant portion, and therefore needs to be reduced using proper shield design. Due to the difference in the physical reaction mechanisms between inelastic gamma and capture gamma, the count rate of inelastic gamma rays remains relatively constant. However, for capture gamma rays, as the boron content increases, the proportional contribution from the formation gradually increases, while the contribution from the tool decreases. For the internal shielding, when the boron content reaches 75%, further increases in boron content no longer significantly affect the count rate, as shown in Fig. 6(a). At this point, the total count response from the formation increases by 2.93%. Therefore, a boron content of 75% is identified as the optimal choice for the internal shielding material.

Additionally, adjusting the boron content in the external shield can achieve more effective shielding as shown in Fig. 6(b). When the external boron content reaches 25%, further increases in boron content do not significantly enhance the shielding effect, with the formation's contribution increasing by 9.56% at this point.

3. *The effect of shielding thickness*

Fig. 6(c) and Fig. 6(d) illustrate the changes in the proportional contributions of capture gamma rays from the formation, tool, mud pipe, and borehole as the thickness of the shielding increases. However, within the internal shielding, the increase in thickness does not significantly increase the formation's contribution to the capture gamma rays, as shown in Fig.6(c), especially compared to the impact of the boron

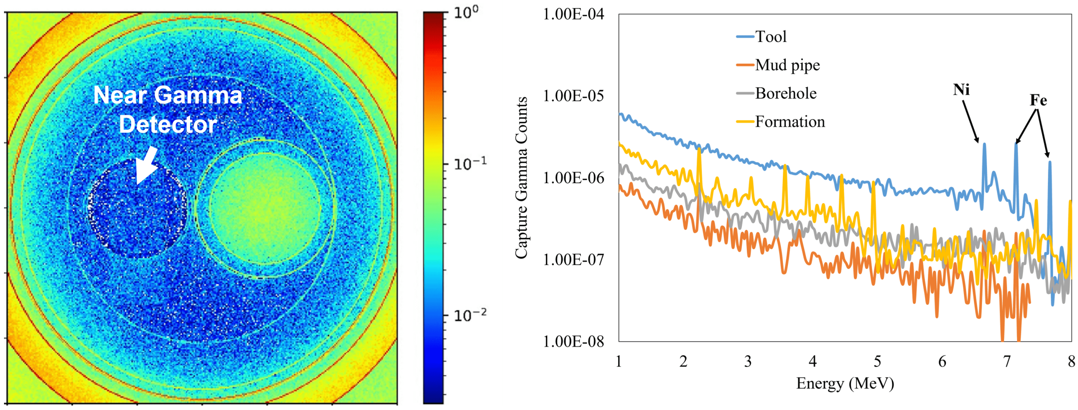

(a) Capture gamma spectra without boron material

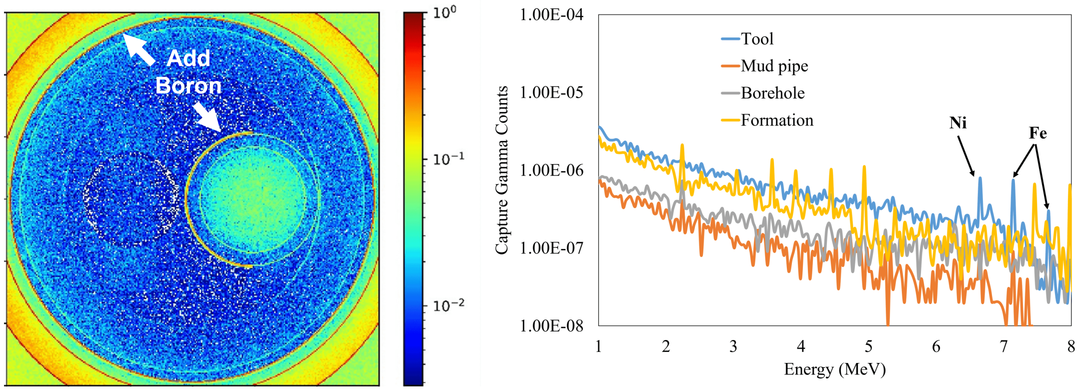

(b) Capture gamma spectra with boron-containing shielding

Fig. 7. Comparative analysis of gamma and neutron distributions with and without shielding

content, as shown in Fig.6(a). Therefore, for this shielding application, employing a method such as spraying boron powder could be a viable option for shielding rather than fabricating a geometric shield.

Fig. 6(d) shows the changes in the gamma contributions of the external shielding increases (thickness varies from 5.2 to 14.2 mm). As the thickness of the external shielding increases, the proportion contributed by the mud pipe decreases approximately proportionally, while the proportion from the formation increases linearly.

The different trends in internal and external shielding are due to the fact that internal shielding primarily prevents thermal neutrons from the mud pipe from entering the tool, and the amount of thermal neutron contribution from the mud pipe is constant. Therefore, with a certain level of shielding, complete shielding of the mud pipe can be achieved. In contrast, external shielding prevents thermal neutrons from the formation from entering the tool. There are more thermal neutrons from formation than from the mud pipe, so the shielding performance increases with the thickness. This indicates that for external shielding, a thicker setup is generally more beneficial. Within the constraints of the tool's size, the maximum thickness of 14.2mm is chosen, at which point the contribution from the formation increases by 5.18%.

4. *Analysis on the gamma spectra*

Fig. 7(a) and Fig. 7(b) illustrate the near gamma detector's X-Y plane distribution and the spectra received by near gamma detector. There is a significant diffusion of thermal neutrons into the tool's interior from outside of the tool and the mud pipe. This would lead to neutron capture by the elements of the tool, thereby generating interference. With the addition of boron to both external and internal shielding, a noticeable reduction in the diffusion of thermal neutrons can be observed, resulting in a lower neutron distribution inside the tool. The increased number of thermal neutrons in both the external and internal shielding indicates enhanced absorption effects of boron.

Besides, the tool is made of stainless steel, containing a high content of Fe and Ni elements. Therefore, without thermal neutron shielding, the gamma spectrum of the tool contains distinct Fe and Ni peaks. The Fe peaks are located at 7.1 MeV and 7.6 MeV; the Ni peak is at 6.6 MeV.In the capture gamma distribution transmitted through the mud pipe, contributions from iron and nickel can also be observed. In terms of count rate contributions, the order is tool > formation > mud pipe > borehole. Therefore, when the contributions from these four sections are combined, the information from formation may be overshadowed by tool information, making it

difficult to analyze formation elements. However, in gamma spectrum after implementing the shielding design, contributions from both the tool and the mud pipe are significantly reduced, demonstrating the effectiveness of the shielding.

IV. CONCLUSION

This study investigated the boron-containing shielding design for a newly developed pulsed neutron logging tool. This manuscript reveals that the mud pipe impact on the detector is significant and cannot be ignored. After fast neutrons are emitted, they get slowed down quickly by water in the mud pipe, resulting in the accumulation of a considerable amounts of thermal neutrons. Since thermal neutrons in the mud pipe do not provide formation information, both neutron and gamma detectors are significantly affected, therefore, advanced shielding strategy is necessary.

Firstly, for neutron detectors, simulation shows that shielding materials with higher boron content such as boron carbide, can achieve improved shielding effect. Considering tool volumetric constraints, the distribution of neutrons, and the performance of shielding thickness, the selected shielding thickness for the near and far neutron detectors are 5mm and 4mm, respectively. From thickness comparison, at a porosity of 25 p.u., the near neutron sensitivity shows a 5.6% increase in response.

Secondly, for the near gamma detector, shielding thermal neutrons is equally important in order to prevent tool-related capture gamma rays produced when thermal neutrons enter the tool. Both internal and external shields are designed. Due to volumetric constraints, internal shield thickness is hard to be adjusted therefore necessitating the use of a high-concentration boron powder coating with 75% boron content. . Meanwhile, the shielding thickness of external shield can be increased and therefore allows more flexibility in design. Simulation shows that the optimal thickness is 14.2mm, with 25% boron content to minimize tool effect. This manuscript could provide references and design insights for the neutron and gamma shielding design of pulsed neutron tools.

---

[1] T. Acheampong, G.A. Kemp. Health, safety and environmental (HSE) regulation and outcomes in the offshore oil and gas industry: Performance review of trends in the United Kingdom Continental Shelf. Saf. Sci., **148**, 105634 (2022).doi: 10.1016/J.SSCI.2021.105634

[2] C. Jiang, V. Herwaarden, Ir. Hans, and Jianwei Peng. "International HSE Standards on China's Largest Gas Project." Paper presented at the SPE International Conference on Health, Safety, and Environment in Oil and Gas Exploration and Production, (Calgary, Alberta, Canada, March 2004). doi: 10.2118/86650-MS

[3] A.J. Gale, U.S. Paent, US3104322A.1958

[4] D.V. Ellis, J.M. Singer, *Well Logging for Earth Scientists*. (Springer, Netherlands, 2007). doi: 10.1007/978-1-4020-4602-5

[5] F. Zhang, S. Hou, X. Jin, Monte carlo simulation on compensated neutron porosity logging in lwd with d-t pulsed neutron generator. Int. J. Appl. Radiat. Isot., **34(3)**, 227-232 (2010). doi: 10.7538/tws.2010.23.01.0015

[6] J.Z Yang. Monte-carlo simulation method in pulsed neutron density logging while drilling. Well Logging Technol., **33(6)**, 521-520 (2009).https://api.semanticscholar.org/CorpusID:124556333

[7] S.A. Scherbatskoy, U.S. Paent, US2648012A.1949

[8] L. Wang, S. Deng, Y. Fan, et al., 2019. Detection performance and inversion processing of logging-while-drilling extra-deep azimuthal resistivity measurements. Petrol. Sci. **16** (5), 1015–1027. doi: 10.1007/s12182-019-00374-4

[9] M. Luycx, T.-V. Carlos, Physics, applications, and limitations of borehole neutron-gamma density measurements. Geophys., **84**, D39–D56. (2019).doi: 10.1190/geo2018-0088.1

[10] J.E. Galford, J.A. Quirein, S. Shannon, et al., Field Test Results of a New Neutron Induced Gamma Ray Spectroscopy Geochemical Logging Tool. Paper presented at the SPE Annual Technical Conference and Exhibition (New Orleans, Louisiana, October 2009). doi: 10.2118/123992-MS

[11] W. Wu, A. Yue, M. Tong, etc., The calculation and characteristic of elemental sensitivity factor in geochemical logging. Pet. Geosci., **21** (1): 74–80. (2014) doi: 10.1144/petgeo2013-049

[12] W. Wu, N. Wei, L. Li, Quantitative analysis of neutron-capture gamma-ray energy spectra using direct demodulation. Pet. Geosci. **79** (2): D91–D98. (2014) doi: 10.1190/geo2013-0296.1

[13] F. Zhang, Q. Zhang, J. Liu, etc., A method to describe inelastic gamma field distribution in neutron gamma density logging, Appl. Radiat. Isot., **129**, 189-195, ISSN 0969-8043 (2017) doi: 10.1016/j.apradiso.2017.08.024

[14] R. Pemper, A. Sommer, P. Guo, et al., A New Pulsed Neutron Sonde for Derivation of Formation Lithology and Mineralogy. Paper presented at the SPE Annual Technical Conference and Exhibition (San Antonio, Texas, USA, September 2006). doi: 10.2118/102770-MS

[15] R. Badry, J. Grau, S. Herron, et al., High-definition spectroscopy determining mineralogic complexity. Oilfield Rev., **26** (1), 34–50 (2014). https://api.semanticscholar.org/CorpusID:53393955

[16] C. Stoller, B. Adolph, M. Berheide, et al., "Use of LaBr3 for downhole spectroscopic applications," 2011 IEEE Nuclear Science Symposium Conference Record (Valencia, Spain, October 2011). doi: 10.1109/NSSMIC.2011.6154477

[17] Q. Zhang, F. Zhang, R. P. Gardner, etc., A method for determining density based on gamma ray and fast neutron detection using a Cs2LiYCl6 detector in neutron-gamma density logging, Appl. Radiat. Isot., **142**, Pages 77-84, ISSN 0969-8043 (2018) doi: 10.1016/j.apradiso.2018.09.011

[18] O. Shcherbakov, F. Furutaka, S. Nakamura, et al. A BGO detector system for studies of neutron capture by radioactive nuclides. Nucl. Instrum. Methods Phys. Res., Sect. A,**517**,1-3 (2003). doi: 10.1016/j.nima.2003.09.042

[19] A.G.C. Nair, R. Acharya, K. Sudarshan, et al., Determination and validation of prompt k(o)-factors with a monochromatic neutron beam at the Dhruva reactor. Nucl. Instrum. Methods Phys. Res., Sect. A, **564**, 2 (2006). doi: 10.1002/1097-4628(20010425)80:4<634::AID-APP1139>3.0.CO;2-

[20] W.Tang, Q. Zhang, A method for neutron-induced gamma spectra decomposition analysis based on Geant4 simulation. Nucl. Sci. Tech., **33**, 154 (2022) doi: 10.1007/s41365-022-01144-5

[21] Y. Wang, Q. Zhang, A characterization study on perovskite X-ray detector performance based on a digital radiography system. Nucl. Sci. Tech., **34**, 69 (2023) doi: 10.1007/s41365-023-01220-4

[22] Q. Liang, F. Zhang, J. Fan, "A Novel Gamma-Thermal Neutron Evaluating Gas Saturation Method Using Pulsed Neutron Logging Tool with Dual-CLYC." Paper presented at the SPWLA 63rd Annual Logging Symposium, (Stavanger, Norway, June 2022). doi:10.30632/SPWLA-2022-0078

[23] Y. Wang, J. Liang, Q. Zhang, "Development and verification of Geant4-based parallel computing Monte Carlo simulations for nuclear logging applications." Ann. Nucl. Energy, **172**, 109079, (2022) doi:10.1016/j.anucene.2022.109079

[24] X. Wang, J. Liang, Y. Li, "Hybrid Monte Carlo methods for Geant4-based nuclear well logging implementation." Ann. Nucl. Energy, **169**: 108824 (2022) doi:10.1016/j.anucene.2021.108824

[25] X. Wang, Q. Zhang, "High-efficiency Monte Carlo simulation based on CADIS method for Gamma Density Measurement." Ann. Nucl. Energy, 185: 109710 (2023).doi:10.1016/j.anucene.2023.109710

[26] Q. Zhang, Source less density measurement using an adaptive neutron induced gamma correction method. Nucl. Sci. Tech., **34**, 125 (2023) doi: 10.1007/s41365-023-01274-4

[27] J. Liu, F. Zhang, X. Wang, et al., 2014. Numerical study on determining formation porosity using a boron capture gamma ray technique and MCNP. Appl. Radiat. Isot. **94**, 266–271. doi: 10.1016/j.apradiso.2014.08.013

[28] Q. Zhang., R. Deng, S. Zhang, et al. An alternative method for sourceless density measurement with boron sleeve gamma detectors. Appl. Radiat. Isot., **174(4)**:109785 (2021) doi: 10.1016/j.apradiso.2021.109785

[29] F. Zhang, W. He, X. Wang, et al., Compact shielding design of a portable 241Am–Be source, Appl. Radiat. Isot., **128**, 49-54 (2017) doi: 10.1016/j.apradiso.2017.06.033

[30] A.M.A. Mostafa, M.H. Zakaly, S.A. Al-Ghamdi, et al., $PbO–Sb_2O_3–B_2O_3–CuO$ glassy system: Evaluation of optical, gamma and neutron shielding properties, *Mater. Chem. Phys.*, **258**, 123937 (2021) doi: 10.1016/j.matchemphys.2020.123937.

[31] M. Rashad, H.A. Saudi, M.H. Zakaly, et al., Control optical characterizations of Ta^{+5}–doped $B_2O_3–Si_2O–CaO–BaO$ glasses by irradiation dose, *Opt. Mater.*, **112**, 110613 (2021) doi: 10.1016/j.optmat.2020.110613.

[32] H.A. Saudi, H.O. Tekin, M.H. Zakaly, et al., The impact of samarium (III) oxide on structural, optical and radiation shielding properties of thallium-borate glasses: Experimental and numerical investigation, *Opt. Mater.*, **114**, 110948 (2021) doi: 10.1016/j.optmat.2021.110948.

[33] Hesham M.H. Zakaly, H.A. Saudi, H.O. Tekin, et al., Glass fabrication using ceramic and porcelain recycled waste and lithium niobate: physical, structural, optical and nuclear radiation attenuation properties, *J. Mater. Res. Technol.*, **15** (2021) doi: 10.1016/j.jmrt.2021.09.138.

[34] J.W. Shin, J.-W. Lee, S. Yu, et al., Polyethylene/boron-containing composites for radiation shielding. Thermochim. Acta, **585**, 5-9 (2014) doi: 10.1016/j.tca.2014.03.039

[35] M.I. Pinilla, A. Hellinger, L.K. Vo, et al., Design studies using MCNP6® for an oil well logging prototype tool and a test facility. Radiat. Phys. Chem., **167**, 108393 (2020) doi: 10.1016/j.radphyschem.2019.108393

[36] E. Calzada, F. Grünauer, B. Schillinger, et al., Reusable shielding material for neutron- and gamma-radiation, Nucl. Instrum. Methods Phys. Res., Sect. A, **651**, 77-80 (2011) doi: 10.1016/j.nima.2010.12.239

[37] J. Allison, K. Amako, J. Apostolakis, et al. GEANT4 - A simulation toolkit. Nuclear Tools and Methods in Physics Research, Nucl. Instrum. Methods Phys. Res., Sect. A, **506(3)**, 250-303 (2004) doi: 10.1016/S0168-9002(03)01368-8

[38] Boralcan, Boralcan American Materials. https://www.americanelements.com/boralcan-al-b4c-matrix-composite

[39] Boron carbide, Boron carbide-Henan Sicheng Abrasives Techo. https://hnabrasive.com/products/Boron carbide.html

[40] K. Ruslan, Mechanical Properties of Boron Carbide (B4C). Electronic Theses and Dissertations, **81** (2020) https://stars.library.ucf.edu/etd2020/81

[41] Aluminum Boron, Master Alloy Supplier | Stanford Advanced Materials. https://www.samaterials.com/aluminum-master-alloy/1622-aluminum-boron-master-alloy.html

[42] S.T. Mileiko, *Chapter II – Fibres and Fibrous Composites*. (Elsevier Science, Moscow, 1997) doi: 10.1016/S0927-0108(97)80020-3